Ore Geology Reviews 158 (2023) 105498

Contents lists available at ScienceDirect

Ore Geology Reviews

journal homepage: www.elsevier.com/locate/oregeorev

Paleozoic VMS-type stratiform mineralization overprinted by Mesozoic vein-type mineralization in the Yushui copper deposit, eastern Guangdong, South China

Gang Chen [a], Maohong Chen [a,*], Changhui Ke [a,*], Yanwen Tang [b]

[a] MNR Key Laboratory of Metallogeny and Mineral Assessment, Institute of Mineral Resources, CAGS, Beijing 100037, China
[b] State Key Laboratory of Ore Deposit Geochemistry, Institute of Geochemistry, Chinese Academy of Sciences, Guiyang 550081, China

ARTICLE INFO

Keywords:
Two stages of mineralization
Vein-type ore body
Superimposed mineralization
Yushui copper deposit
South China

ABSTRACT

The South China hosts a number of stratiform deposit in Late Paleozoic depression, including the Yushui copper deposit (which has a Cu grade up to 53% with an average grade of about 3.5%) in the Yong-Mei-Hui depression. The genesis type of Yushui copper ore is highly controversial due to the influence of post mineralization tectonic and magmatic activities, which affects the exploration of the deposits. Yushui copper deposit is mainly composed of stratiform ore body and stockwork orebody in the footwall, with typical VMS-type deposit characteristics and its mineralization age of 308 Ma. Small amounts of vein-type ore body can also be seen in the hanging wall dolomite of the stratiform ore body, which mainly develops along the joints and faults, and the mineral assemblage includes chalcopyrite, bornite, galena, sphalerite, tetrahedrite, furutobeite, and rare earth minerals (xenotime and bastnaesite). Hydrothermal sericite is also developed when vein-type ore body cut the sandstone in the footwall of stratiform ore body. Pristine euhedral xenotime and bastnaesite crystals from the Yushui Cu mineralized of veins ore body yield LA-ICP-MS weighted mean $^{206}Pb/^{238}U$ ages of 162.5 ± 6.7 Ma (1 s, MSWD = 11.8) and 164.6 ± 5.3 Ma (1 s, MSWD = 9.5), respectively. Hydrothermal sericite yields a plateau ^{40}Ar–^{39}Ar age of 163.19 ± 7.60 Ma, which is consistent with the xenotime and bastnaesite U–Pb age, suggesting that the vein-type Cu mineralized is generically related to the Middle-Late Jurassic hydrothermal event. These ages indicate that in addition to the major Late Paleozoic mineralization events that formed VMS-type stratiform ore body, there were also small-scale hydrothermal vein-type ore body formed during the Middle and Late Jurassic mineralization events that did not cause major disruptions to the earlier stratiform ore body. Combining with the chronological research of other copper deposits in the southeastern coastal area of China, this article believes that these 170 ~ 155 Ma deposits were all due to the crust-mantle interaction caused by changes in the subduction angle of the ancient Pacific plate. Our study suggests that the southeastern margin of the South China has potential for the exploration of polymetallic hydrothermal mineralization related to Middle-Late Jurassic magmatic rock.

1. Introduction

The Yushui copper deposit is located within the Late Palaeozoic Yong-Mei-Hui depression in South China and is characterised by the prevalence of stratiform copper-rich ore bodies (He, 1990; Zhao et al., 2021; Chen et al., 2021; Liu et al., 2023). A series of Carboniferous-controlled stratiform copper-bearing sulfide deposits (e.g. Yushui, Makeng etc.) developed within the depressional zone (Han and Ge, 1983; Yang et al., 2017; Zhao et al., 2021). The ore bodies of these deposits are of interest due to their unique stratigraphically-controlled, stratiform output, with some ore bodies and mineral phases reflecting sedimentary features, but many of the important deposits have suffered alteration by later tectonic/magmatism event in South China (Gu et al., 2007; Zaw et al., 2007; Zhu et al., 2016; Qiu et al., 2018). As a result, their genesis has been a focus of debate in scholarship for nearly half a century (Xu and Zhou, 2001; Mao et al., 2009; Hou et al., 2011; Jiang et al., 2011; Chen and Yang, 2021).

Several different opinions have been put forward on the genesis of the Yushui copper deposit, including submarine volcanic-associated massive sulfide deposits (He, 1990; Chen et al., 2021), sedimentary

* Corresponding authors.
E-mail addresses: mhchen666@163.com (M. Chen), kechanghuicags@126.com (C. Ke).

https://doi.org/10.1016/j.oregeorev.2023.105498
Received 23 March 2023; Received in revised form 3 May 2023; Accepted 21 May 2023
Available online 25 May 2023

exhalative and late superimposed (Wang et al., 1999; Huang et al., 2015), magmatic hydrothermal (Chen et al., 1994), The Mississippi Valley-type (MVT) (Cheng et al., 2014; Jiang et al., 2014; Jiang, 2016) and Sandstone-type Copper ore (SSC) (Liu et al., 2023). Field studies have demonstrated that Yushui copper deposit is mainly stratiform ore body, but it has been affected by later tectonic-magmatic events (Gu et al., 2007), forming a small number of vein-type ore body, prompting the need for a new understanding of its genesis.

In this study, we use detailed field observations, xenotime and bastnaesite U-Pb ages, and sericite ^{40}Ar-^{39}Ar age to constrain the timing of vein-type mineralization. Based on a synthesis of our research results and previous studies of mineralization ages of stratiform ore body, we reconstruct the formation and evolution of the deposits and strengthen the genetic link between vein-type Cu and magmatic hydrothermal in the region, guiding the exploration of similar deposits in the region.

2. Regional Geology

Late Palaeozoic tectonic settings of South China is characterised by widespread extension and fault depression zones formation, such as the Middle-Lower Yangtze, the Qiantang River-Xinjiang, the Xianggui-Yuebei and Yong-Mei-Hui fault depression zones (Gu et al., 2003). Subsidence of all these depression zones is thought to be related to the break-up and rifting of the South China block from Gondwana (Zaw et al., 2007). In the period from the Devonian to the Middle Triassic, all depression zones generally received several thousand metres of sediments, predominantly of carbonates and clastic rocks (Xu and Zhu, 1978). Many copper deposits are developed in these depressional zones, and the genesis of the deposits is highly controversial.

The Late Palaeozoic Yong-Mei-Hui depression is developed between the two faults, and the Yushui copper deposit is located in the middle of the depression (Bureau of Geology and Mineral Resource of Guangdong, 1988; Huang et al., 2015). The Yushui copper deposit, located at the continental margin of South China, is separated from the Cathaysia Block by the Zhenghe–Dapu Fault to the southeast (Fig. 1), Shaowu–Hengyuan Fault to the northwest.

The region strata exposed include pre–Devonian metamorphic, Late Paleozoic–Middle Triassic clastic sedimentary and carbonate rocks, and Mesozoic–Cenozoic continental clastic and volcanic rocks (Shu et al., 2009).

The tectonics in the area is mainly NE-trending region fault, three fault control the distribution of magmatic rocks in the area (Xu, 1993; Xu et al., 2000), especially in the intersection of NE-trending fractures, NW and EW-trending secondary fractures often develop volcanic basins, granitic rocks and their related deposit.

The intrusive rocks in the area are mainly formed at 170–155 Ma and 145–130 Ma (Liu et al., 2018; Jia et al., 2018). The early stage instrusions are mainly high potassium calc-alkaline quartz diorite and granodiorite, and the genetic type is I-type granite, which is related to the mineralisation of porphyry Cu/Cu-Au deposits in the area (Jia et al., 2018; Mao et al., 2021; Bao et al., 2021). The main lithologies in the later stages are monzonitic granite, moyite, biotite granite and granite porphyry, all of which are highly fractionated and closely related to the mineralisation of tin (tungsten) deposits (Chen et al., 2008; Qiu et al., 2017; Liu et al., 2018).

3. Deposit Geology

The Yushui copper deposit, located about 15 km NE of in Meizhou city in eastern Guangdong Province (Fig. 2), was discovered in the 1980 s, with underground mining in progress since the 1985 s. The proven metal reserves include 102,100 tons Cu with an ore grade of 3.5%, 186,600 tons Pb with an ore grade of 1.5%, 117,600 tons Zn with an ore grade of 1.3% and 339 tons Ag.

The exposed strata in the mining area mainly consist of Middle to Upper Devonian ($D_{2\text{-}3}$) clastic rocks, Lower Carboniferous Zhongxin Formation (C_1z) clastic rocks, Middle to Upper Carboniferous ($C_{2+3}ht$) carbonate rocks, and overlying unconformably Upper Jurassic Gaojiping

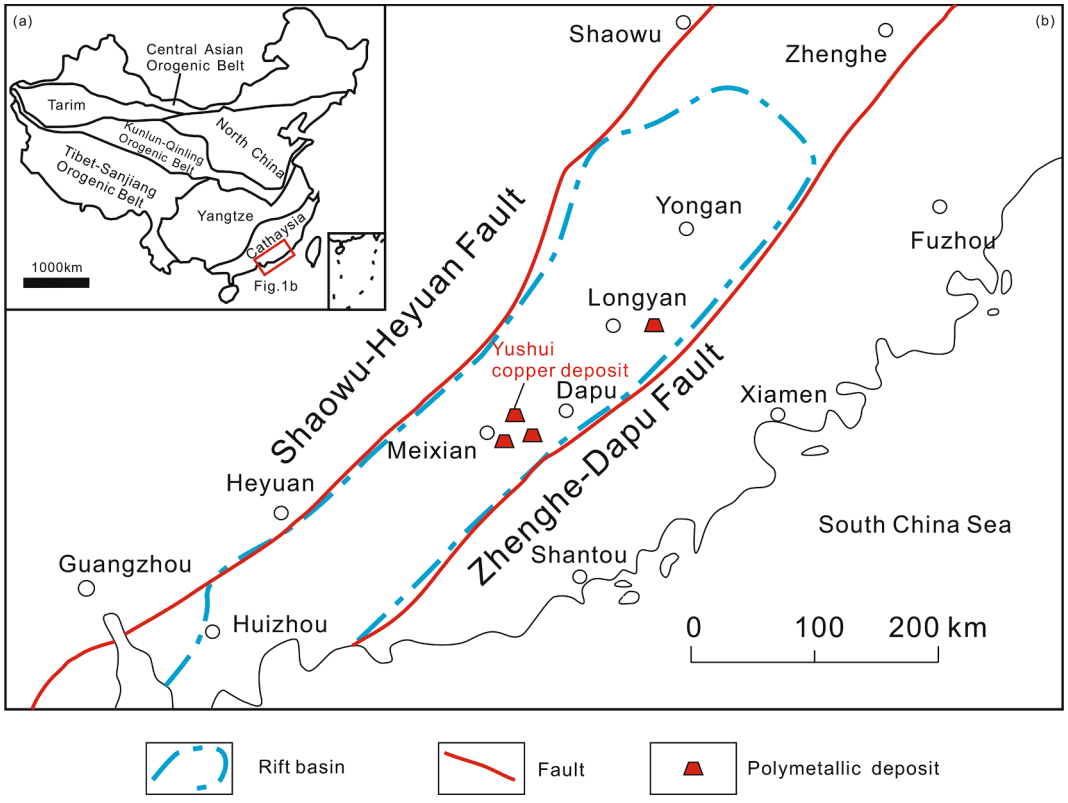

Fig. 1. Regional geological map of Yong'an-Meizhou-Huizhou depression district. Modified from He (1990).

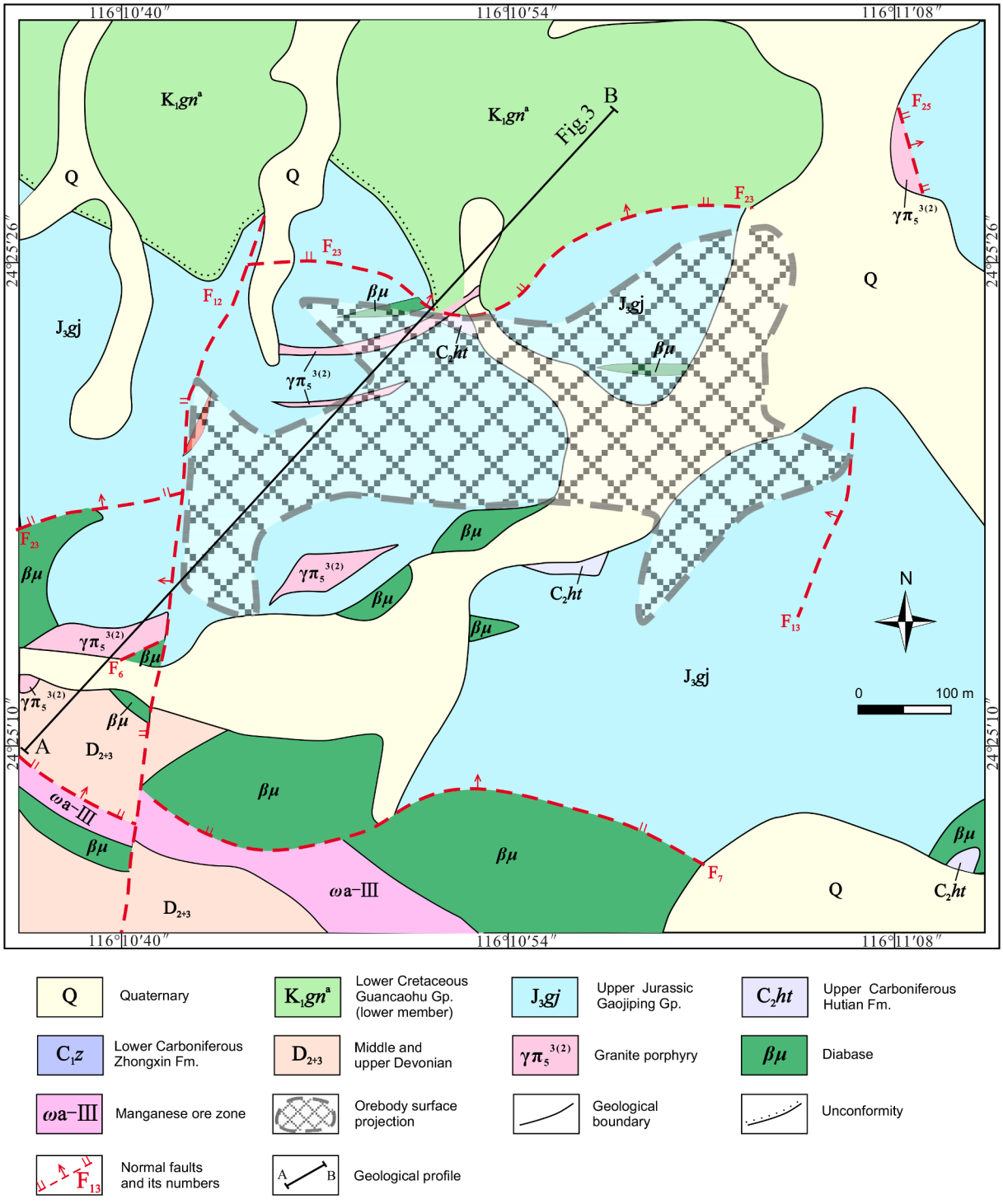

Fig. 2. Geological map of the Yushui deposit.Modified from 723 Geological team of the Bureau of Geology and Mineral Resources of Guangdong Province (GTBGMRG), 1988.

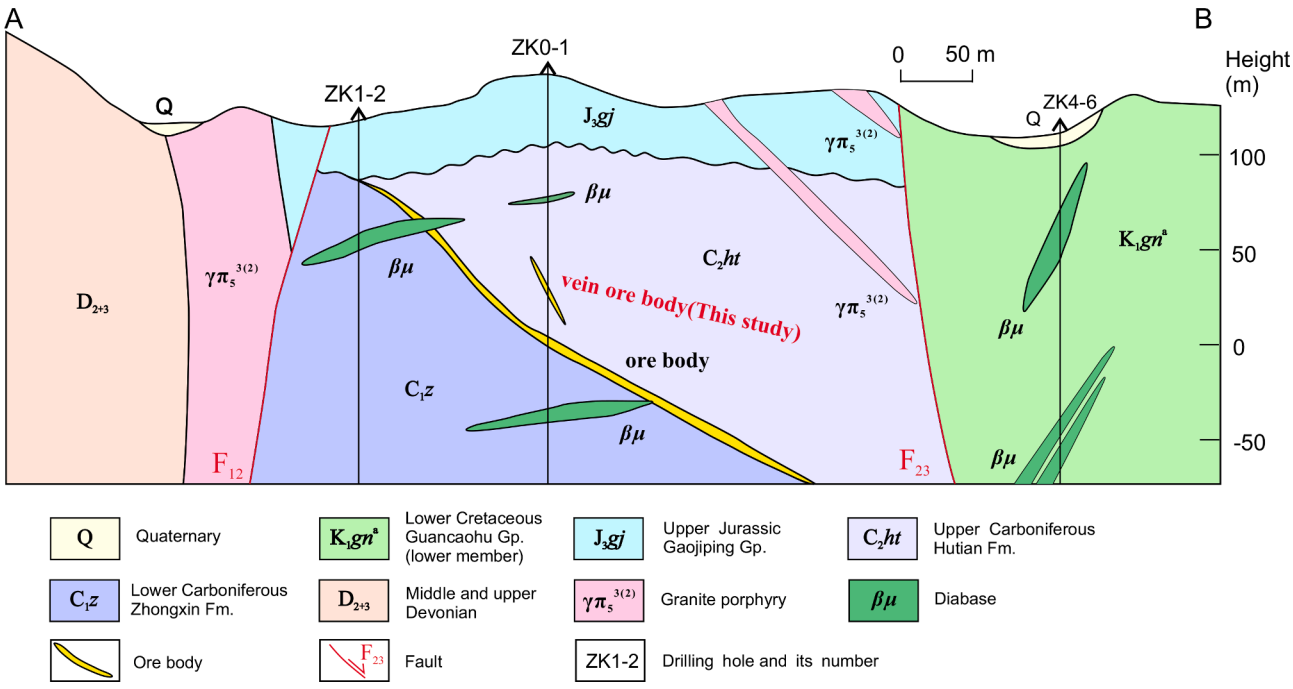

Fig. 3. Geological section of exploration line a-b. See Fig. 2 for location of geological section. Modified from He (1990).

group(J_3gj) continental volcanic rocks, Lower Cretaceous (K_1gn^a) inland lake volcanic-sedimentary rocks, and Quaternary (Q) deposits, etc(Fig. 2).

Both the Devonian and Carboniferous strata show NE-dipping monoclinic structures (Fig. 3). Local normal/transtensional faults are NNE-trending or nearly EW-trending, and are part of the controlling structures for the Yanshanian volcanic basin.

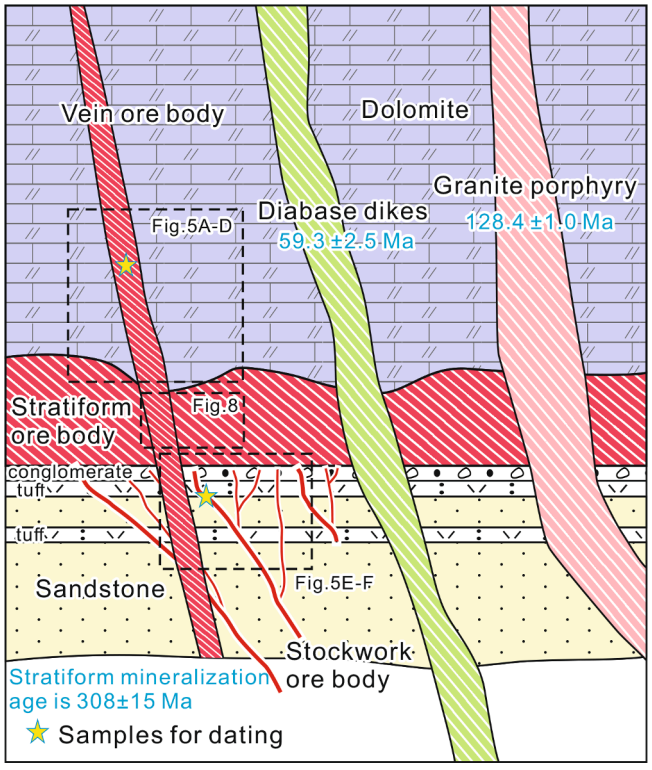

Fig. 4. Idealized model of vein-type mineralization in the Yushui copper deposit(dotted rectangles indicate the locations shown in the other panels) (modified from Chen et al., 2021).

Local magmatic rocks include mainly Yanshanian dikes of different sizes (outcrop size: 20 ~ 300 cm wide) and shapes, including those of granite porphyry, quartz porphyry and diabase. The intrusions clearly cut the stratiform ore body along straight boundary. Xenoliths of limestone and orebodies are present in the dykes, indicating that the dikes are post-ore. Li (2019) reported LA-ICP-MS zircon U-Pb ages of the granite-porphyry (128.4 Ma) and diabase (59.3 Ma).

The Yushui copper deposit is divided into two types of ore bodies (Fig. 3). The main ore body (stratiform ore body) is distributed roughly along the interface between the C_2ht dolomite and the C_1z quartz sandstone, appearing stratiform or quasi- stratiform and clearly demarcated from the surrounding rocks. The alteration is strong in the footwall, not at in the hanging wall. The ore body exhibits the characteristic of being thick in the middle and thin at the edges. Detailed geological characteristics are presented in Chen (2021) and consider the Yushui copper deposit as a VMS-type deposit.

The Vein-type ore body generally appear on the hanging wall of the stratiform ore body and are connected to the stratiform ore body at their roots (Figs. 4, 5A). The Vein-type ore body cut along the bedding plane along joints and faults and extend upwards for only about 2 ~ 10 m. The Vein-type ore body are about 5 ~ 40 cm thick, with chalcopyrite dominated distributed in a lens in the middle and bornite on both sides (Fig. 5B). Stockwork bornite mineralization occurs in the white marble on both sides of the vein, which is locally wedge-shaped and fills the joints, with a width of about 20 cm (Fig. 5C). The vein-type ore body is nearly vertical, trending at 265°, suggesting that the orebody was formed by filling along joints. A wide alteration zone (such as marbleized) appears on both sides of the vein, with its boundary controlled by joints. Silicification and mineralization occur near the boundary, appearing as disseminated and vein lead–zinc mineralization (Fig. 5D).

The chalcopyrite in the vein-type ore body is replacemented by pyrite and hematite. It contains a small amount of galena, sphalerite, tetrahedrite. (Fig. 6A). The bornite ores is mainly composed of bornite, chalcopyrite, galena, sphalerite, hematite and REE minerals (Fig. 6B-D), with calcite and quartz as inclusions (Fig. 6E). The adjacent sulfide stockwork vein are mainly composed of sphalerite (Fig. 5F), which dissolves chalcopyrite (Fig. 6G). The edge is composed of galena, bornite, and a small amount of covellite (Fig. 6H). Furutobeite and

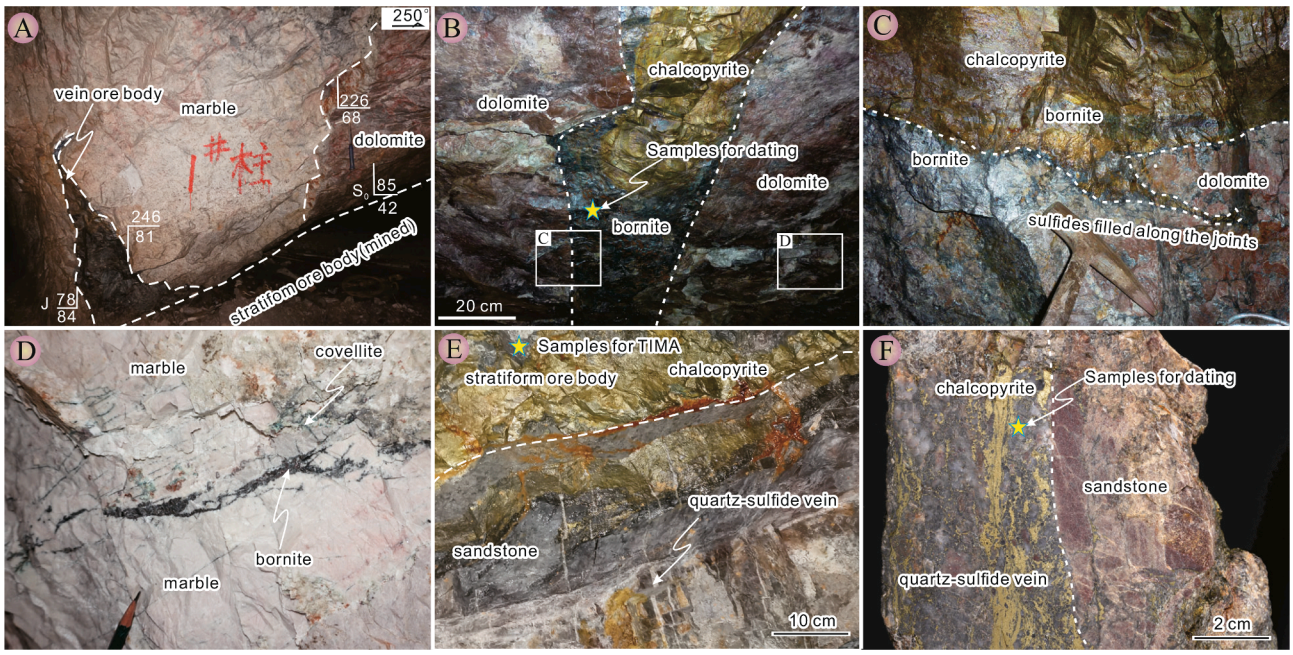

Fig. 5. Representative photos of ores in the Yushui copper deposit. A-Vein-type ore body filled along joints; B-chalcopyrite + boenite vein cut the bedding of dolomite; C-Sulfides filles along the joints; D-The surrounding rocks exhibit vein mineralization in the distal area; E- Quartz-sulfide veins in the lower part of stratiform ore body; F- The boundary between quartz-sulfide veins and surrounding rocks is clear.

bornite are distributed between the particles of the dolomite.

When the vein-type ore body cuts the sandstone, ore body is limited by joints on both sides, composed of gray-green sulfide-rich (chalcopyrite, bornite) strongly altered sandstone, strongly silicified, sericitized, and chloritized, which is clearly distinguished from the purple-red quartz surrounding rock (Fig. 5.E-F). Under the microscope, secondary enlargement of quartz grains, disseminated and vein chalcopyrite, and a small amount of galena can also be seen (Fig. 6I). The notable feature of vein-type ore body is the exceptionally diverse mineral species and complex paragenetic assemblages. By observing a large variety of different types of minerals using polarizing microscopes and scanning electron microscopes, it has been established that vein-type ore body can be divided into four stages of mineralization, with a detailed sequence of mineral generation shown in Fig. 7. Xenotime and bastnaesite do not have obvious light and dark variations, and both contain each fine inclusions, indicating that they are coeval and show the same stage with the bornite (Fig. 7).

4. Sampling and analytical methods

4.1. Sampling

Representative samples were collected from the stratiform ore body, hanging wall vein-type ore body and quartz-sulfide vein in the sandstone. These samples (dating minerals of REE and sericite), their characteristic (Fig. 5), and their mineral assemblages (Figs. 6-7) have been described previously. Samples were examined by standard optical microscopy using transmitted and reflected light to study paragenetic relationships. The selection of the sericite was carried out at the Langfang Tuoxuan Rock and Mineral Testing Service Co., Ltd, Hebei Province, China.

4.2. Analytical methods

4.2.1. TESCAN Integrated mineral Analyzer (TIMA) analysis

The bornite ore sample was selected from the stratiform ore body for TIMA analysis where it cross cut with vein-type ores (Fig. 5E, 8A). Mineral compositional mapping were obtained on carbon-coated thin sections (mounts) using a MIRA3 scanning electron microscope equipped at Guangzhou Tuoyan Analytical Technology Co., Ltd. We use an acceleration voltage of 25 kV, probe current of 8.29nA. Working distance was set to 15 mm. Pixel spacing was set to 1 μm and dot spacing was set to 3 μm. The current and BSE signal intensity were calibrated on a platinum Faraday cup using the automated procedure. EDS performance was checked using manganese standard. The samples were scanned using TIMA liberation analysis module.

4.2.2. EPMA analyses

Mineral compositions were determined at the MNR Key Laboratory of Metallogeny and Mineral Assessment, Institute of Mineral Resources, Chinese Academy of Geological Sciences, with a JEOL JXA-iHP200F Electron Probe Micro Analyzer (EPMA) equipped with five wavelength-dispersive spectrometers. Details of EPMA methods are described in Yang et al. (2022). During the analysis, an accelerating voltage of 20 kV, a beam current of 20nA and a 1 μm spot size were used to analyze minerals. Natural minerals and alloy were used as standards. Data were corrected on-line using a modified ZAF (atomic number, absorption, fluorescence) correction procedure.

4.2.3. Xenotime and bastnaesite LA-ICP-MS U-Pb dating

U-Pb dating of xenotime and bastnaesite was carried out by LA-*sf*-ICP-MS in the State Key Laboratory of Deposit Geochemistry, Institute of Geochemistry, Chinese Academy of Sciences. The laser ablation system is GeoLasPro 193 nm ArF excimer laser. For low-U minerals (≤10 ppm), in order to improve the accuracy of age, element XR high-resolution magnetic mass spectrometry (ICP-MS)(Thermo Fisher Scientific, USA) produced by thermoelectric company was used to analyze the age separately. In the process of laser ablation, helium carrier gas and argon gas are used as compensation gas.Low U mineral analysis needs to add a small amount of nitrogen to improve sensitivity. Two/three gases are mixed through a T-joint before entering ICP. The sample chamber is a standard denudation tank, in which a mold made of resin is added to obtain a smaller volume of sampling space to reduce the memory effect and improve the flushing efficiency. In the analysis process, the laser working parameters are generally frequency ~ 5 Hz, energy density 3–4 J/cm^2, beam spot 16–44 μm(the actual situation depends on the U-Pb content in the sample).

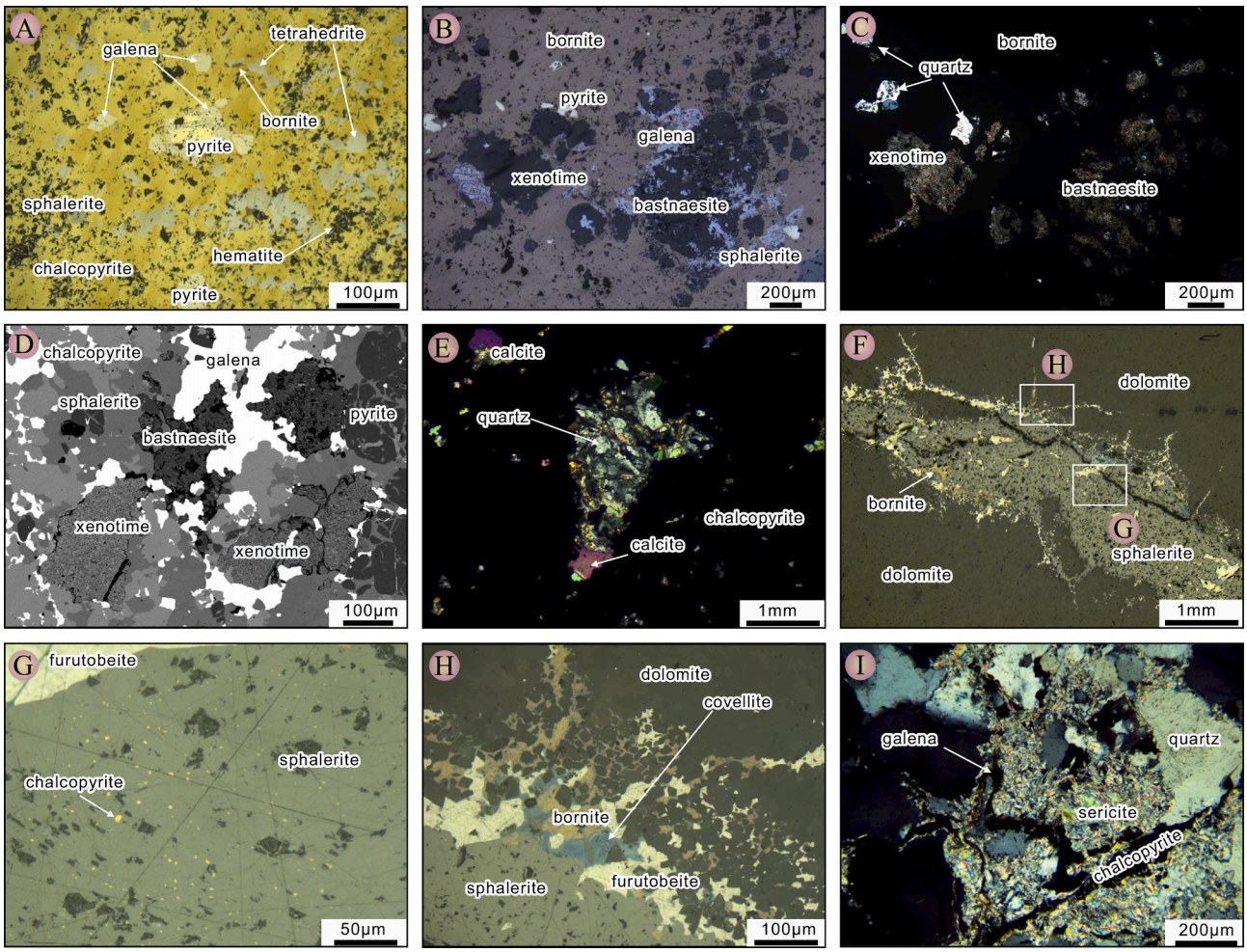

Fig. 6. Representative micrograph of ores in the Yushui copper deposit. A-The chalcopyrite is replacemented by pyrite and hematite, and coexists with bornite, tetrahedrite, galena, pyrite and sphalerite; B-D Bornite and rare earth minerals coexist(reflected light, cross-polarized light, and BSE respectively); E- The hydrothermal quartz and calcite in the bornite; F-Vein mineralization at the contact zone of the surrounding rock; G-Dissolution of chalcopyrite in sphalerite; H-The covellite, chalcopyrite, and galena in the contact zone of the surrounding rock; I-Hydrothermal sericite in stockwork ore body.

The performance of ICP-MS was optimized with SRM610 or 612 prior to testing to achieve the best sensitivity and ionization efficiency (U/Th≈1), the smallest possible oxide yield (ThO/Th < 0.3%) and low background values.

The off-line processing of analytical data (including the selection of samples and blank signals, instrument sensitivity drift correction, element content and U-Th-Pb isotope ratio and age calculation) was performed using the software ICPMS DataCal (Liu et al., 2008; Liu et al., 2010). In U-Pb isotopic dating, the standard sample XN01 or XN-02 (Vasconcelos et al., 2018) was used for isotope fractionation correction, and each analysis of 10 sample points, analysis of two standard samples. For the U-Th-Pb isotope ratio drift related to the analysis time, the change of the standard sample was corrected by linear interpolation (Liu et al., 2010). Phosphoyttriite XN-05 or Zagi and bastnaesite MNP and Zagi were used as quality control samples for analysis. Isoplot (Ludwig, 2003) was used to draw the U-Pb age harmonic diagram and calculate the age weight average.

4.2.4. Sericite Ar-Ar dating

The samples were crushed and sieved to 40–60 mesh, and picked under a binocular microscope to ensure the purity of muscovite was greater than 99%. The samples were then ultrasonically cleaned and sealed in quartz bottles for neutron irradiation. Irradiation was conducted in the “swimming pool reactor” at the China Institute of Atomic Energy using the D10 channel for a total irradiation time of 2160 min. Standard samples were also irradiated for monitoring purposes, including the ZBH-25 black mica standard with a standard age of 132.7 ± 1.2 Ma and a K content of 7.6%. The samples were heated in a graphite furnace in stages, with each stage being heated for 10 min and purified for 20 min. Mass spectrometry analysis was performed on a multi-collector rare gas mass spectrometer GV Helix MC, with 20 data sets collected for each peak. All data were corrected for mass discrimination, atmospheric argon, blank, and interference element isotopes after regressing to time zero. Correction factors for interference isotopes generated during neutron irradiation were obtained by analyzing irradiated K_2SO_4 and CaF_2, with values of $(^{36}Ar/^{37}Aro)Ca = 0.0002398$, $(^{40}Ar/^{39}Ar)K = 0.004782$, $(^{39}Ar/^{37}Aro)Ca = 0.000806$. ^{37}Ar was corrected for radioactive decay, with a decay constant of $\lambda = 5.543 \times 10^{-10}$ $year^{-1}$ for ^{40}K. Plateau ages and forward and reverse isochrons were calculated using the ArArCALC program (Koppers, 2002), with plateau age errors given at 2 s. For a detailed experimental process, please refer to the relevant articles (Chen et al., 2006; Zhang et al., 2006).

5. Results

5.1. Mineralogy of TIMA

The TIMA counts the mineral content of the sample. It contains with 86.44% bornite, 2.48% galena, 2.29% quartz, 1.68% sphalerite, 1.58% pyrite, 0.55% xenotime, 3.27% bastnaesite and minor chalcopyrite,

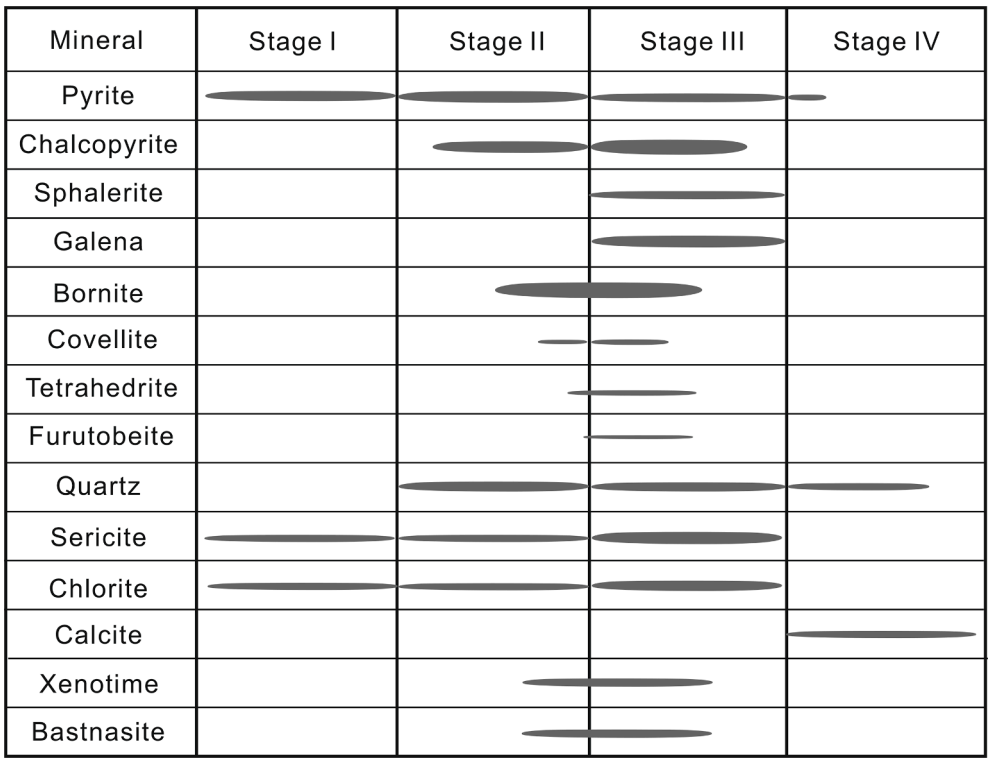

Fig. 7. Paragenetic sequence of vein ore body in the Yushui copper deposit.

siegenite and anhydrite. Pyrite is obviously replaced by bornite. REE minerals are developed along the late fractures of bornite (Fig. 8B-C). The mineral assemblages of vein-type ore body exhibit pronounced differences from stratiform ore body. Vein-type ore body are enriched in furutobeite (Fig. 6G-H), which are consistent with the coexistence of galena and REE minerals (Fig. 8C), implying the introduction of metal elements in the later stage.

5.2. Geochemical compositions of xenotime and bastnaesite

The composition of xenotime and bastnaesite grains from the Yushui copper deposit are shown in Table 1. Xenotime contains with 32.11 to 33.58 wt% P_2O_5, 0.24 to 0.72 wt% UO_2, 0.38 to 0.48 wt% PbO, 60.33 to 63.21 wt% ΣREE(O), 0.14 to 0.24 wt% CaO, 0 to 0.14 wt% F and 0.17 to 0.73 wt% FeO. Bastnaesite consistent with 0 to 6.89 wt% P_2O_5, 0 to 0.13 wt% UO_2, 0 to 0.04 wt% ThO_2, 0.25 to 0.80 wt% PbO, 53.50 to 58.07 wt % ΣREE(O), 7.71 to 18.62 wt% CaO, 2.15 to 4.71 wt% F and 0.04 to 0.44 wt% FeO.

5.3. Xenotime and bastnaesite U-Pb ages

U-Pb isotope data for 13 analyses on 13 xenotime grains are summarized in Table 2. The calculated U-Pb ages are presented in Fig. 9a. Fourteen analyses define a Tera-Wasserburg lower intercept age of 162.5 ± 6.7 Ma (1 s, MSWD = 11.8).

U-Pb isotope data for 49 analyses on 25 bastnaesite grains are summarized in Table 3. The calculated U-Pb ages are presented in Fig. 9b. Thirty analyses on eight bastnaesite grains define a Tera-Wasserburg lower intercept age of 164.6 ± 5.3 Ma (1 s, MSWD = 9.5).

5.4. Sericite Ar-Ar ages

The ^{40}Ar-^{39}Ar analytical results for sericite from the Yushui deposit (sample YSB-9) are presented in Table 4 and illustrated in Fig. 10. The age spectra show a flat plateauwith 96.7% of ^{39}ArK released, indicating that K and radiogenic ^{40}Ar in the sample are distributed homogeneously, and that K-Ar isotopic systematics were not affected by heating disturbances over the geological history of the sample. Six continuous steps

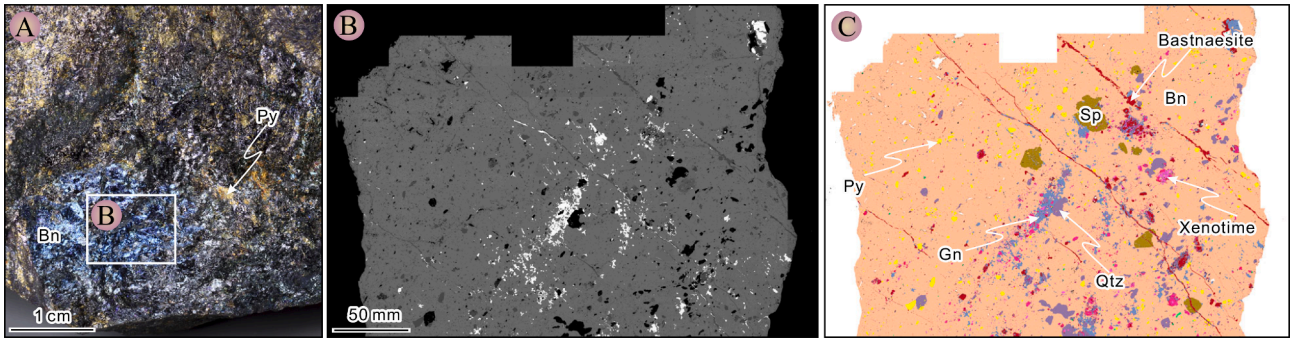

Fig. 8. TESCAN Integrated Mineral Analyzer (TIMA) mineral phase map showing relationships between bornite, galena, pyrite, sphalerite, xenotime and bastnaesite. Abbreviations: Bn = bornite, Gn = galena, Sp = sphalerite, Py = pyrite, Qtz = quartz.

Table 1
EMPA data for xenotime and bastnaesite from the Yushui copper deposit.

Content (wt.%)	Xe-1	Xe-2	Xe-3	Xe-4	Xe-5	Ba-1	Ba-2	Ba-3	Ba-4
mineral	xenotime					bastnaesite			
F	0.04	0.06	0.00	0.03	0.14	3.94	4.71	2.15	3.07
SiO_2	0.60	0.12	0.24	0.41	0.90	0.12	0.00	0.10	0.00
Ta_2O_5	0.06	0.04	0.09	0.00	0.02	0.01	0.00	0.00	0.07
CaO	0.16	0.23	0.24	0.14	0.20	16.05	15.79	7.71	18.62
P_2O_5	32.95	33.11	33.20	33.58	32.11	1.13	0.01	6.89	0.00
La_2O_3	0.00	0.00	0.00	0.00	0.01	0.19	0.31	0.21	0.26
Y_2O_3	40.27	38.98	39.69	38.94	39.40	31.70	31.68	32.07	30.13
ThO_2	0.00	0.00	0.00	0.00	0.00	0.00	0.02	0.02	0.04
UO_2	0.49	0.24	0.36	0.33	0.72	0.00	0.05	0.13	0.00
Nb_2O_5	0.00	0.00	0.00	0.00	0.00	0.00	0.04	0.00	0.00
FeO	0.59	0.42	0.17	0.60	0.73	0.14	0.44	0.27	0.04
Ce_2O_3	0.00	0.00	0.00	0.00	0.06	1.90	3.78	1.62	3.32
Tb_2O_3	0.83	0.71	0.30	0.70	0.44	0.00	0.00	0.00	0.00
Yb_2O_3	8.53	9.97	7.67	10.17	9.15	0.71	0.33	3.12	0.15
Ho_2O_3	0.74	1.52	1.27	1.26	1.11	1.91	1.95	2.03	2.11
Lu_2O_3	1.59	2.03	1.55	1.77	1.60	0.82	0.40	1.26	0.69
TiO_2	0.00	0.00	0.00	0.03	0.00	0.00	0.02	0.00	0.00
Tm_2O_3	0.91	0.68	0.31	0.72	0.38	1.99	0.39	0.18	0.00
Pr_2O_3	0.00	0.12	0.00	0.03	0.07	0.40	0.85	0.40	0.55
Nd_2O_3	0.08	0.10	0.13	0.03	0.04	3.72	5.73	2.45	5.05
Sm_2O_3	0.00	0.00	0.00	0.00	0.00	0.89	1.75	1.24	1.52
Gd_2O_3	0.13	0.19	0.22	0.14	0.24	2.59	4.10	3.10	3.43
Dy_2O_3	2.73	2.90	3.08	2.47	2.60	4.89	4.96	4.97	5.22
Er_2O_3	5.70	5.68	5.56	5.52	5.43	1.39	1.09	3.92	1.00
HfO_2	0.29	0.29	0.46	0.23	0.23	0.46	0.69	0.56	0.00
PbO	0.40	0.47	0.48	0.38	0.48	0.33	0.80	0.34	0.25
Total	97.08	97.83	94.99	97.46	96.00	73.60	77.90	73.85	74.20

Table 2
LA-ICP-MS xenotime(Sample YS-55-X) U-Pb dating results in the Yushui copper deposit.

Sample No.	Signal value (cps)			Isotope ratio					
	Pb	Th	U	$^{207}Pb/^{206}Pb$	1σ	$^{207}Pb/^{235}U$	1σ	$^{206}Pb/^{238}U$	1σ
YS55-X-19	91.164	2.088	151.017	0.723	0.012	18.562	0.343	0.187	0.003
YS55-X-24	60.621	1.349	108.708	0.693	0.013	16.925	0.489	0.177	0.004
YS55-X-25	110.846	3.010	151.007	0.736	0.011	22.304	0.417	0.220	0.003
YS55-X-26	211.202	2.226	3061.296	0.316	0.006	1.623	0.036	0.037	0.001
YS55-X-27	137.367	3.593	1663.732	0.356	0.006	2.012	0.035	0.041	0.001
YS55-X-35	309.024	2.304	6622.988	0.179	0.009	0.806	0.055	0.032	0.001
YS55-X-36	170.570	2.930	1575.690	0.415	0.009	2.986	0.108	0.052	0.001
YS55-X-38	70.497	1.598	131.863	0.684	0.014	16.437	0.497	0.175	0.005
YS55-X-52	81.913	4.419	143.651	0.715	0.016	17.501	0.329	0.179	0.003
YS55-X-56	187.051	2.062	2294.155	0.370	0.007	2.249	0.067	0.043	0.001
YS55-X-59	81.013	0.000	76.880	0.757	0.012	32.360	0.570	0.311	0.005
YS55-X-60	98.396	0.121	92.391	0.754	0.013	32.389	0.479	0.313	0.004
YS55-X-61	66.017	0.000	72.457	0.786	0.012	29.070	0.487	0.270	0.004
YS55-X-9	102.492	3.774	167.171	0.741	0.011	19.175	0.405	0.188	0.003

(650–800 °C) of one sericite sample yield a well-defined weighted plateau age of 163.19 ± 7.60 Ma (MSWD = 24.23) (Fig. 10). The initial $^{40}Ar/^{36}Ar$ ratio is close to the atmospheric value (295.5, Steiger and Jager, 1977), indicating no excess argon in the sample. Therefore, the plateau age of 163.19 ± 7.60 Ma is believed to be reliable estimates of the crystallization age of sericite.

6. Discussion

6.1. Age of vein mineralization

The U-Pb geochronology of hydrothermal xenotime and bastnaesite has been demonstrated to be a powerful and reliable tool for constraining the age of polymetallic mineral deposits (Rasmussen et al., 2007; Liu et al., 2011; Yang et al., 2014; Ling et al., 2016; Feng et al., 2022), and recent studies have found that xenotime and bastnaesite can eliminate matrix effects in dating(Tang et al., 2022). The structures of xenotime and bastnaesite are uniform, well-formed and compositionally stable in the vein-type ore body (Table 1). They are intergrown with each other, and the vein-type copper mineralization shows a synchronous co-precipitation relationship with xenotime and bastnaesite (Fig. 6. B-D).

This study obtained U-Pb ages of xenotime and bastnaesite in vein-type mineralization from the upper part of the stratiform ore body, which yielded ages of 162.5 ± 6.7 Ma (1σ, MSWD = 11.8) and 164.6 ± 5.3 Ma, respectively. The age of the stratiform ore body has been previously determined by bornite and chalcopyrite Re-Os dating as 308 Ma (Huang et al., 2015) and our unpublished hematite U-Pb age (320 ± 15 Ma) and dolomite Sm-Nd age (308.1 ± 4.6 Ma), and it has been demonstrated to have a sedimentary exhalative origin.

The stcokwork mineralization in the lower part of the stratiform ore body is considered to be the fluid channel of sedimentary exhalative, and the both form a double-layered mineralized structure (Fig. 4). In this study, an Ar-Ar age of 163.19 ± 7.60 Ma was obtained from sericite in the boundary between stcokwork ore body and vein-type ore body (Fig. 4). The large gap between the ages of the stcokwork and stratiform ore bodies is speculated to be another hydrothermal or thermal resetting event. Previous studies have measured homogenization temperatures of

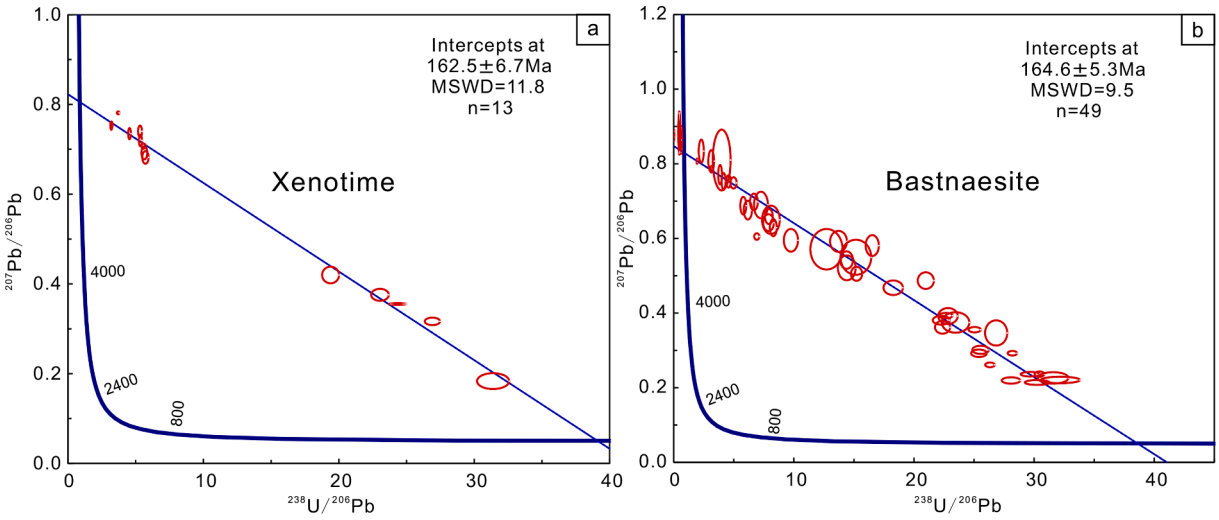

Fig. 9. Representative Tera-Wasserburg diagrams and corresponding weighted mean plots of age data for hydrothermal xenotime and bastnaesite from the Yushui copper deposit.

quartz fluid inclusions in stcokwork ore bodies (fluid channels) more than 200 °C (91–289 °C and 77–267 °C) (Jiang, 2016; Huang, 2015), presumably for multiple generations of fluid inclusions, implying that the ^{40}Ar-^{39}Ar age of sericite may be a later hydrothermal age (Li et al., 2022).

The ^{40}Ar-^{39}Ar age of sericite and the ages of xenotime and bastnaesite in the vein ore body are consistent within the error range, indicating a single hydrothermal mineralization event in the Middle-Late Jurassic. The S isotope results from previous studies indicate that the ore-forming materials were partly derived from seawater (-2.4 ~ 1.0 ‰) (sedimentary exhalative origin) and partly contributed by mantle-derived magma (Huang, 2015). The samples with mantle-derived contributions is vein-type ore body, located in carbonate rocks in the hanging wall (sample numbers: Rz1 and YS027, ^{34}S: 1.00 ~ 2.60 ‰) (He, 1990), suggesting that the vein-type ore body ore-forming materials may have originated from this event (163 Ma). In addition, representative massive bornite ores from the stratiform ore body were selected for TIMA scanning, which clearly shows that the later REE bands cut through the stratiform ore body (Fig. 4,8).

The ore-forming age of the stratiform ore body is 308 ± 15 Ma (Huang et al., 2015; Chen et al., unpublished). The difference in ore-forming time between the stratiform and vein-type ore body indicates that they are the products of two different ore-forming events in the Yushui copper deposit. Xenotime and bastnaesite are the main minerals in the South China(Eastern Guangdong and southern Jiangxi) weathering crust ion-adsorbed REE deposit (Xie et al., 2016; Xu et al., 2017; Zhao et al., 2022), and most of the rare earth parent rocks that contain these minerals have ages concentrated around 160 Ma (Li et al., 2017; Li et al., 2019b), indicating the existence of a magmatic-hydrothermal event containing REE and copper in the Middle-Late Jurassic.

6.2. *Genesis of the Yushui deposit and its implications*

6.2.1. *Significance of superimposed mineralization*

Superimposed metallogenic systems are commonly formed in long and complex ore-forming processes due to the superimposition of different ore-forming events (Zhai et al., 2009). Superimposed mineralization has been reported in many mineralized zones in China (Jiang et al., 2010, 2011; Li et al., 2019a), including more than twenty major stratiform deposits in South China such as Wushan, Chengmenshan, Xinqiao, Yongping, Dabaoshan, and Fankou. These deposits occur in several Hercynian-Indian depression basins, which some consider to be typical skarn-type and/or magmatic-hydrothermal vein-type ores (Pan and Dong, 1999; Mao et al., 2009). However, others believe they were formed by seafloor sedimentation and then intruded by Mesozoic granite intrusions and associated hydrothermal fluids, leading to superimposition, transformation, and modification (Zhou and Li, 2000; Zaw et al., 2007; Gu et al., 2007). The disagreement on the genesis of these deposits is due to the clastic basins of the Late Paleozoic, which may have resulted in boiling and immiscibility of fluids when the depth of seawater is < 1500 m, leading to the formation of less sulfides (usually vein-type and stockwork but not stratiform) (Herzig and Hannington, 1995; Ni et al., 2005; Mao et al., 2009). However, fluid boiling could also contribute to metal precipitation at/near the seafloor in shallow-water hydrothermal systems (Hannington, 2021; Falkenberg et al., 2021; Schaarschmidt et al., 2021). The discovery of carbonate mud mounds, fluid channel, *syn*-volcanic faults, and contemporaneous volcanic rock provides strong evidence of exhalative sedimentary mineralization (Ni et al., 2005; Jiang et al., 2011; Guo, 2010). In South China, large-scale skarnization caused difficulties in establishing the genesis of the deposits due to multi-phase magmatic activity during the Yanshanian (Zhai et al., 2009; Chang et al., 2012). However, the Yushui copper deposit, which has only undergone minor modification, preserves primary features such as fluid channel, *syn*-volcanic faults, contemporaneous volcanic rock, and exhalites that are important for discussing the genesis and evolution of superimposed mineralization (Chen et al., 2021).

The current study confirms the presence of Middle-Late Jurassic vein-type mineralization. The Middle-Late Jurassic magmas may have followed the same tectonic path as the Late Paleozoic submarine hydrothermal systems, resulting in the coexistence of massive sulfide with vein-type, skarn, and porphyry ore bodies in the same area or in a single deposit (Gu et al., 2007). Both primary stratiform ore body and Middle to Late Jurassic vein ore body are present in the Yushui copper deposit (Chen et al., 2021). So, the unmodified stratiform ore body at the Carboniferous interface in the region could serve as mutual prospecting criteria with the Late Paleozoic stratiform ore bodies and Middle-Late Jurassic vein-type ore body. However, it is unclear whether the supernormal Cu enrichment in the Yushui copper deposit is linked to superposition mineralization.

6.2.2. *Implications for vein-type mineralization*

The Late Mesozoic magmatism in the South China region is widely considered to be associated with the active continental margin along the coastal area (Zhou et al., 2006; Li et al., 2007; Li and Li, 2007; Meng et al., 2012). In recent years, a large amount of intrusive volcanic rock

Table 3
LA-ICP-MS bastnaesite(Sample YS-55-B) U-Pb dating results in the Yushui copper deposit.

Sample No.	Signal value (cps)			Isotope ratio					
	Pb	Th	U	$^{207}Pb/^{206}Pb$	1σ	$^{207}Pb/^{235}U$	1σ	$^{206}Pb/^{238}U$	1σ
YS55-B-1	65.955	2.924	359.816	0.580	0.016	4.848	0.188	0.061	0.001
YS55-B-10	137.612	1.634	1557.491	0.377	0.019	2.203	0.128	0.043	0.001
YS55-B-11	19.429	2.049	143.889	0.537	0.032	4.999	0.396	0.066	0.004
YS55-B-12	13.270	4.695	61.161	0.604	0.027	5.953	0.275	0.073	0.002
YS55-B-13	48.077	4.170	902.498	0.238	0.007	1.098	0.027	0.034	0.001
YS55-B-14	49.373	4.319	311.071	0.505	0.012	4.579	0.146	0.066	0.001
YS55-B-16	87.617	1.611	129.208	0.753	0.012	22.763	0.717	0.219	0.006
YS55-B-17	59166.562	2.851	746.393	0.881	0.018	2519.811	66.745	20.827	0.513
YS55-B-2	111.228	3.104	159.241	0.567	0.037	16.384	0.592	0.173	0.005
YS55-B-20	284348.342	2.317	152.587	0.882	0.017	58514.732	2445.731	486.342	19.873
YS55-B-21	256.323	2.829	5081.353	0.215	0.006	0.976	0.029	0.033	0.001
YS55-B-22	50.970	0.921	137.268	0.657	0.014	11.472	0.390	0.126	0.003
YS55-B-23	95.874	1.444	146.051	0.748	0.011	20.736	0.762	0.201	0.007
YS55-B-28	104.245	1.897	290.715	0.640	0.012	11.227	0.497	0.127	0.005
YS55-B-29	195.267	2.330	2690.588	0.299	0.005	1.628	0.049	0.039	0.001
YS55-B-3	8921.697	4.917	930.462	0.795	0.029	264.385	32.008	2.173	0.246
YS55-B-30	12.177	3.929	93.369	0.476	0.019	3.532	0.142	0.055	0.002
YS55-B-31	11.889	2.331	243.775	0.229	0.012	0.988	0.051	0.032	0.001
YS55-B-32	1372.471	0.497	214.715	0.846	0.022	196.121	18.687	1.646	0.150
YS55-B-33	40.099	0.242	109.108	0.630	0.018	10.461	0.348	0.121	0.003
YS55-B-34	280.411	7.993	6054.120	0.220	0.005	0.946	0.040	0.031	0.001
YS55-B-37	223.584	6.507	3440.135	0.292	0.004	1.430	0.024	0.035	0.000
YS55-B-39	202.579	2.290	3130.265	0.261	0.004	1.369	0.026	0.038	0.000
YS55-B-4	132.003	4.999	1526.175	0.357	0.009	2.232	0.081	0.045	0.001
YS55-B-40	210.321	1.874	3897.115	0.217	0.004	1.078	0.034	0.036	0.001
YS55-B-41	164.344	2.102	2432.966	0.289	0.006	1.587	0.045	0.039	0.001
YS55-B-42	124.962	1.575	1222.402	0.391	0.007	2.394	0.049	0.044	0.001
YS55-B-43	89.430	3.081	318.761	0.588	0.014	8.414	0.440	0.103	0.004
YS55-B-44	47.174	3.380	269.894	0.519	0.020	4.990	0.270	0.069	0.002
YS55-B-45	141.403	2.494	1777.144	0.355	0.005	1.957	0.037	0.040	0.001
YS55-B-46	69.403	5.052	87.060	0.757	0.026	25.033	0.823	0.241	0.006
YS55-B-47	122.127	2.752	138.470	0.767	0.014	27.565	0.966	0.259	0.007
YS55-B-48	104.300	3.324	333.596	0.639	0.015	11.077	0.792	0.124	0.007
YS55-B-49	83.760	3.011	55.512	0.831	0.021	50.191	3.268	0.436	0.026
YS55-B-5	110.722	3.251	120.851	0.760	0.039	28.005	3.920	0.251	0.031
YS55-B-50	52.206	3.910	544.500	0.383	0.012	2.358	0.069	0.045	0.001
YS55-B-51	166.389	5.107	3057.755	0.236	0.005	1.071	0.024	0.033	0.000
YS55-B-53	42.143	2.074	231.800	0.543	0.017	5.195	0.195	0.070	0.002
YS55-B-54	125.334	2.926	1484.837	0.383	0.009	2.369	0.102	0.044	0.001
YS55-B-55	68.495	2.487	160.055	0.611	0.012	12.071	0.276	0.145	0.003
YS55-B-57	62.757	3.256	754.831	0.336	0.017	1.781	0.122	0.037	0.001
YS55-B-58	50.210	4.246	102.736	0.676	0.019	15.105	0.666	0.162	0.006
YS55-B-62	57.558	0.573	127.117	0.676	0.015	13.106	0.823	0.138	0.007
YS55-B-63	136.170	0.946	313.420	0.689	0.012	14.421	0.556	0.150	0.005
YS55-B-66	134.334	0.354	1003.683	0.514	0.013	6.194	0.582	0.079	0.005
YS55-B-67	126.577	0.203	69.851	0.810	0.013	57.350	0.806	0.515	0.007
YS55-B-68	76.450	0.000	68.954	0.790	0.013	34.598	0.586	0.319	0.005
YS55-B-7	147.295	2.356	1324.272	0.443	0.014	3.201	0.118	0.048	0.001
YS55-B-64	141.645	0.245	127.016	0.802	0.015	35.707	1.986	0.321	0.016

Table 4
^{40}Ar-^{39}Ar stepwise heating data for serocote (Sample YSB-9) from the Yushui copper deposit.

	T	40Ar/39Ar	1σ	37Ar/39Ar	1σ	36Ar/39Ar	1σ	40(r)/39(k)	1σ	Age	1σ	40Ar(r)	39Ar(k)
1	600℃	72.414526	0.184305	0.000000	0.086380	0.089991	0.002713	45.82098	± 1.61480	134.76	± 4.58	63.28	2.42
2	650℃	62.767851	0.107212	0.000000	0.011095	0.037326	0.000450	51.73647	± 0.31760	151.45	± 0.89	82.43	13.67
3	680℃	62.873380	0.102583	0.000000	0.008443	0.014081	0.000358	58.71084	± 0.28528	170.93	± 0.79	93.38	15.87
4	710℃	62.037720	0.102685	0.016116	0.008248	0.011660	0.000288	58.59263	± 0.25796	170.60	± 0.72	94.45	17.94
5	740℃	60.459633	0.099304	0.000505	0.006470	0.009984	0.000244	57.50777	± 0.23764	167.59	± 0.66	95.12	19.68
6	770℃	58.840047	0.096126	0.046916	0.006658	0.017642	0.000359	53.63077	± 0.27475	156.76	± 0.77	91.14	15.17
7	800℃	58.995317	0.102410	0.003086	0.020539	0.028919	0.000659	50.44839	± 0.42638	147.83	± 1.20	85.51	7.28
8	840℃	56.095872	0.130469	0.104266	0.041243	0.046637	0.001480	42.32465	± 0.89516	124.83	± 2.55	75.44	3.75
9	940℃	52.243147	0.118243	0.000000	0.049822	0.069575	0.001300	31.68247	± 0.77607	94.24	± 2.25	60.64	2.62
10	1400℃	127.916806	0.360502	0.000000	0.070686	0.376775	0.003800	16.57905	± 2.15873	49.93	± 6.41	12.96	1.60

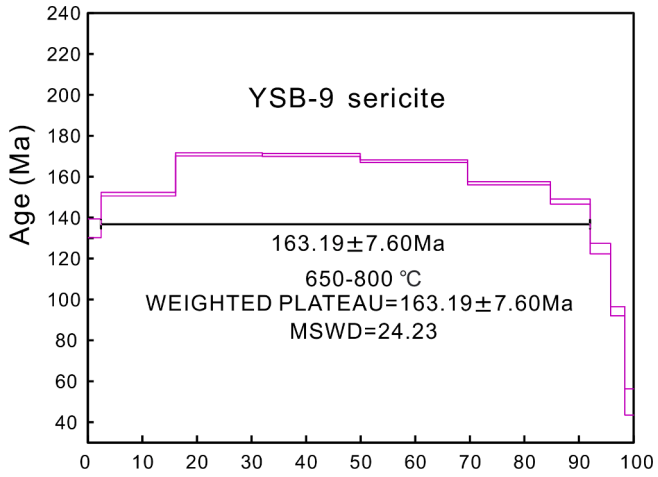

Fig. 10. Sericite ^{40}Ar-^{39}Ar plateau age of the Yushui copper deposit.

Table 5
Age summary of the Middle-Late Jurassic Cu mineralization and related igneous rocks in South China.

Deposit/Igneous	Rock/Mineral	Age(Ma)	Method	Source
Yushui copper deposit	chalcopyrite + bornite	308 ± 15	Re-Os	Huang et al, 2015
Yushui copper deposit	hematite	320 ± 15	LA-ICP-MS U-Pb	Chen et al., unpublished
Yushui copper deposit	dolomite	308.1 ± 4.6	Sm-Nd	Chen et al., unpublished
Yushui copper deposit	Xenotime	162.5 ± 6.7	LA-ICP-MS U-Pb	This study
Yushui copper deposit	Bastnaesite	164.6 ± 5.3	LA-ICP-MS U-Pb	This study
Yushui copper deposit	Sericite	163.19 ± 7.6	Ar-Ar	This study
Xinliaodong quartz diorite	zircon	161 ~ 160	LA-ICP-MS U-Pb	Wang, 2015
Zhongqiuyang rhyolite tuff	zircon	164.7	LA-ICP-MS U-Pb	Jia et al 2020a
Honggoushan rhyolite porphyry	zircon	161	LA-ICP-MS U-Pb	Fan et al., 2018
		161.7 ± 7.5	LA-ICP-MS U-Pb	Gao et al., 2018
E'di biotite granite	zircon	169.4	LA-ICP-MS U-Pb	Liu, 2018
Donggang granodiorite porphyry	zircon	165.5 ± 2.5	LA-ICP-MS U-Pb	Jia et al., 2020b
Gutian, Fujian	molybdenite	162.4 ± 3	Re-Os	Li et al., 2016
	zircon	158.0–161.4	LA-ICP-MS U-Pb	Tian, 2020
Tongcun, Zhejiang	molybdenite	162	Re-Os	Zhang et al., 2013
	Sericite	155.5	Ar-Ar	Liu 2018
Linghou, Zhejiang	molybdenite	162.2 ± 1.4	Re-Os	Tang et al., 2017
	zircon	160.6	LA-ICP-MS U-Pb	Tang et al., 2017
Gaojiping Group	zircon	162–156	LA-ICP-MS U-Pb	Yue et al., 2022

dating data have been published, which are concentrated in the time period of 190–80 Ma, with three peaks at 170–155 Ma, 145–130 Ma, and 110–90 Ma (Mao et al., 2013; Liu, 2018). Due to the tearing and melting of the Izanagi subducting plate, adakitic granodiorite (porphyry) and related porphyry-skarn copper-polymetallic deposits(such as the Qin-Hang metallogenic belt) were formed, with their mineralization and magmatism occurring between 175 and 160 Ma (Mao et al., 2013).

In recent years, Middle-Late Jurassic porphyry Cu-Au-(Mo) deposits have also been discovered in the southeastern coastal areas. A series of Middle-Late Jurassic(170–155 Ma) Cu mineralizations have developed along the Zhenghe-Dafu fault, such as the Xinliaodong, Zhongqiuyang, and Honggoushan copper-polymetallic deposits in eastern Guangdong, the Gutian Cu-Mo deposit in western Fujian, and the Tongcun and Linghou Cu-Au deposits in Zhejiang (Table 5). They are inferred to have formed in an active continental margin environment under the background of subduction (Wang et al., 2016; Jia et al., 2020b). The recent discovery of A_2-type granites (165 Ma) (Zhongqiuyang rhyolitic tuff) confirms that the eastern Guangdong area was in a subduction-related continental margin arc tectonic environment during the middle-late Jurassic (Jia, 2018).

The peak of the magmatic event in eastern Guangdong occurred in the Middle-Late Jurassic (170–154 Ma) and the early Cretaceous (146–132 Ma) (Liu, 2018; Jia, 2018; Ke, 2021). The volcanic rocks are mainly rhyolites, and the intrusive rocks are mainly quartz monzonites, granodiorites, and granites, with a small amount of mafic dykes (Fig. 11 and reference). The magma source is mainly composed of older crustal material with a small amount of younger components. With the continuous subduction, local extension and faulting occurred in the intracontinental.

During the Middle-Late Jurassic period (175–152 Ma), the angle of subduction of the ancient Pacific plate changed, causing upwelling of the asthenosphere mantle and partial melting of the crust, forming the felsic magma mixed with mantle material, which upwelled along the Zhenghe-Dapu Fault and erupted to form the volcanic rocks of the Gaojiping Formation and granodiorite porphyry(Wang, 2015). The vein-type ore body of Yushui copper deposit was formed at the same period as the overlying Gaojiping Formation volcanic rocks, and the latter has higher contents of Cu, Pb, and Zn(51.2 ppm Cu, 26.44 ppm Pb, 71 ppm Zn) (Qiu et al., 2017; Yue et al., 2022), implying that the formation of the vein-type ore body of the Yushui copper deposit is related to contemporaneous magmatic activity. However, we cannot completely rule out the involvement of a small amount of metals leached from the overlying late Paleozoic stratiform ore during the ascent of magmatic fluid.

The deposits listed in Table 5 appear to have a connection, to varying degrees, with underlying or surface magmatic rocks. Based on this observation, it is hypothesized that the middle-late Jurassic magmatic rocks flanking the Zhenghe-Dafu fault represent promising targets for copper exploration. To support this hypothesis, we propose a regional mineralization model (Fig. 12). Notably, prior investigations of the eastern Guangdong region did not identify any copper mineralization in the western section of the Zhenghe-Dapu fault. Thus, our age-of-mineralization study fills a significant research gap in this area.

7. Conclusions

1 Xenotime and bastnaesite Tera-Wasserburg ages of an Cu mineralized vein from the Yushui deposit point to Paleozoic VMS-type stratiform mineralization overprinted by Mesozoic vein-type mineralization in the Eastern Guangdong region(Southeastern Coastal Metallogenic Belt).

2 The Southeast margin of the South China has potential for the exploration of polymetallic hydrothermal mineralization related to Middle-Late Jurassic magmatic rock.

Declaration of Competing Interest

The authors declare that they have no known competing financial interests or personal relationships that could have appeared to influence the work reported in this paper.

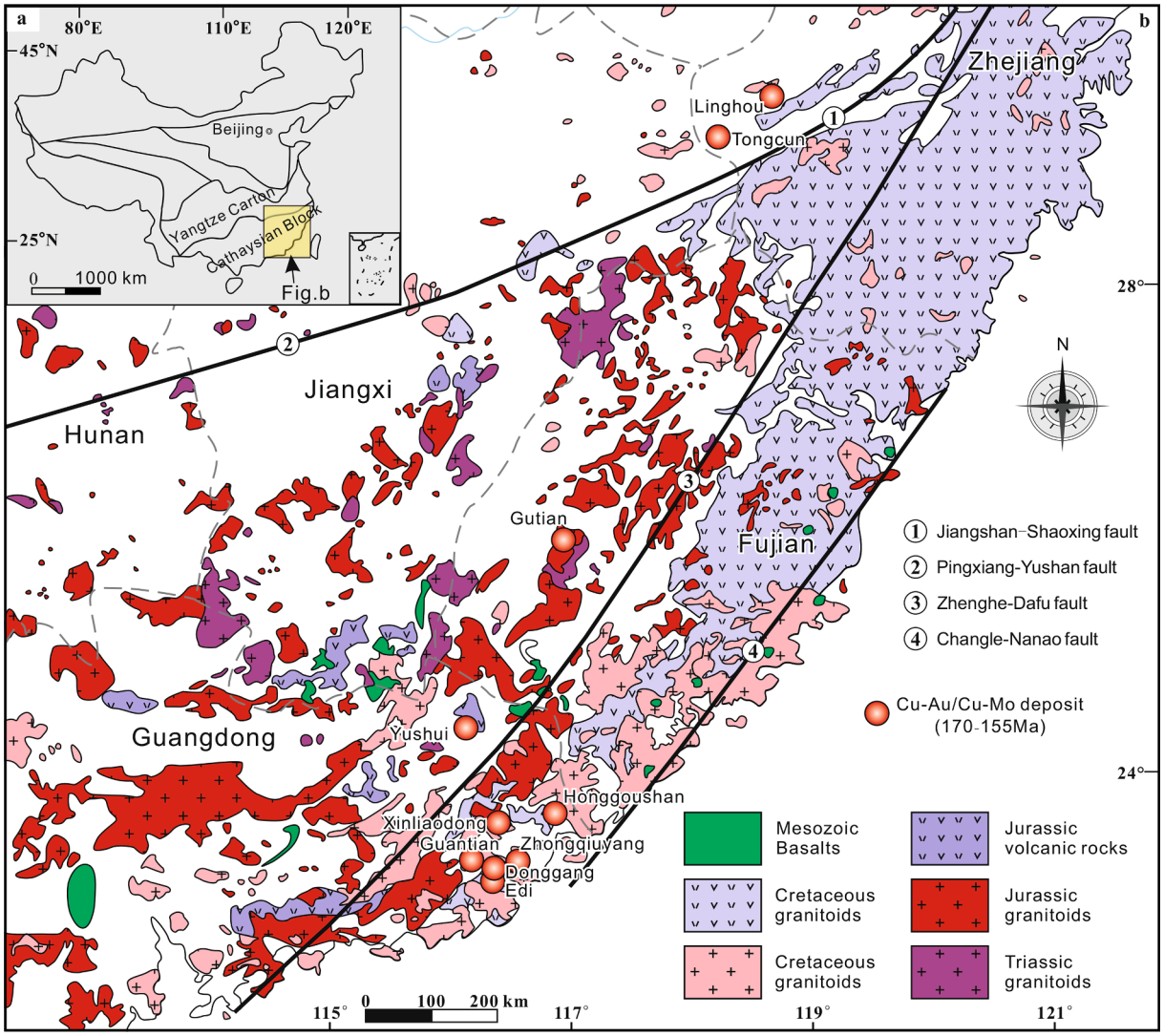

Fig. 11. Reported ages for the SE China Cu-Au-Mo mineralization (modified from Jia et al., 2018).

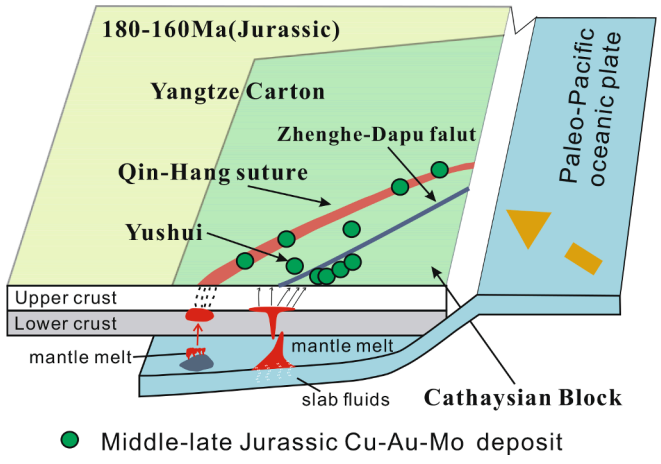

Fig. 12. Schematic diagram showing the Jurassic tectonic evolution of the Southern China and the geodynamic setting of Yushui copper deposit (modified from Jia et al., 2018).

Data availability

Data will be made available on request.

Acknowledgments

Editor Huayong Chen, and two reviewers are thanked for constructive reviews that greatly improved the quality of this paper. We thank Dr. Yongfei Tian and Kezhong Ma, and local geologist Wei Zhang and Yongxin Peng for providing assistance during field investigation. Thanks to Profs Bernd Lehmann, Larry Meinert and Richard Goldfarb for their guidance and comments during the field trips of the Yushui copper deposit. We express our appreciation to Profs. Zhenyu Chen, Chunhua Liu and Junjie Han for their help with data collection. We are indebted to Dr. Wenhao Tang for their suggestions on the manuscript draft. Appreciation is also extended to Dr. Junzeng Zuo for improving the English in this manuscript. This research was financially supported by the National Natural Sciences Foundation of China (42072110) and the mineral survey project of China Geological Survey (DD20201173).

References

Bao, T., Ni, P., Wang, G.-G., Dai, B.-Z., Chen, H., Fan, F.-P., Li, S.-N., Chi, Z., Zhu, R.-Z., Fan, M.-S., 2021. Petrogenesis of the Late Jurassic Cu-Mo mineralization-related Xianyang granite porphyry in the Dehua district, Southeast China: Response to the subduction of paleo-Pacific slab and implication for regional exploration. Lithos 402-403, 106254.

Bureau of Geology and Mineral Resource of Guangdong, 1988. Regional Geologu of Guangdong Province. Beijing: Geological Publishing House, 795–825 (in Chinese).

Chang, Y.F., Zhou, T.F., Fan, Y., 2012. Polygenetic compound mineralization and tectonic evolution: Study in the MiddleLower Yangtze River Valley metallogenic belt. Acta Petrologica Sinica 28 (10), 3067–3075 in Chinese with English abstract.

Chen, B.H., Guo, R., Yu, S.Y., 1994. Metallogenic features and genesis of Cu-polymetallic deposit of Yushui field. Guangdong. Geology and Exploration 23 (03), 20–25.

Chen, M., Ke, C., Tian, Y., Chen, G., Ma, K., Ma, S., Peng, Y., Zhang, W., 2021. Sedimentary-exhalative massive sulfide deposits in shallow marine environment: a case study from Yushui copper deposit, Guangdong Province. Acta Geologica Sinica 95, 1774–1791 in Chinese with English abstract.

Chen, C.-H., Lee, C.-Y., Shinjo, R., 2008. Was there Jurassic paleo-Pacific subduction in South China?: Constraints from 40Ar/39Ar dating, elemental and Sr–Nd–Pb isotopic geochemistry of the Mesozoic basalts. Lithos 106 (1-2), 83–92.

Chen, Y.X., Yang, D., 2021. Research progress on genesis of stratabound sulfide deposits in Tongling ore concentration area of Middle and Lower Yangtze River metallogenic belt. Mineral Deposits 40, 128–142 in Chinese with English abstract.

Chen, W., Zhang, Y., Zhang, Y.Q., Jin, G.S., Wang, Q.L., 2006. Late Cenozoic episodic uplifting in southeastern part of the Tibetan plateau evidence from Ar-Ar thermochronology. Acta Petrologica Sinica 22 (4), 867–872.

Cheng, X., Zhu, X., Wang, Y., Wang, H., Jiang, B., 2014. Genesis of Yushui Copper polymetallic deposit in Meizhou, Guangdong Province. Mineral Deposits 33, 373–374 in Chinese with English abstract.

Falkenberg, J.J., Keith, M., Haase, K.M., Bach, W., Klemd, R., Strauss, H., Yeo, I.A., Rubin, K.H., Storch, B., Anderson, M.O., 2021. Effects of fluid boiling on Au and volatile element enrichment in submarine arc-related hydrothermal systems. Geochimica et Cosmochimica Acta 307, 105–132.

Fan, F., Xiao, H., Chen, L., Li, H., Cai, Y., Kang, C., Zhu, Y., Liu, J., Deng, Z., Li, S., Lin, G., Zhou, X., Xiao, F., 2018. SHRIMP Zircon U-Pb Dating, Lu-Hf Isotopic Composition of Rhyolitic Porphyry in Honggoushan Gold Deposit, Eastern Guangdong, and Their Geological Significance. Geological Review 64, 213–226 in Chinese with English abstract.

Feng, H., Shen, P., Zhu, R., Zi, J.-W., Groves, D.I., Li, C., Wu, Y., Ma, G., Li, T., 2022. Precise ages of gold mineralization and pre-gold hydrothermal activity in the Baiyun gold deposit, northeastern China: in situ U-Pb dating of hydrothermal xenotime and rutile. Mineralium Deposita 57, 1001–1022.

Gao, F., Huang, H., Zeng, Z., Fang, L., 2018. Geological characteristics and metallogenic regularity of gold silver polymetallic deposit in Honggoushan, Guangdong. Mineral Exploration 9, 374–380 in Chinese with English abstract.

Gu, L., Khin, Z., Hu, W., Zhang, K., Ni, P., He, J., Xu, Y., Lu, J., Lin, C., 2007. Distinctive features of Late Palaeozoic massive sulphide deposits in South China. Ore Geology Reviews 31, 107-138.

Gu, L.X., Hu, W.X., Ni, P., He, J.X., Xu, Y.Y., Lu, J.J., Lin, C.M., Li, W.Q., 2003. New Discussion on the South China-type massive sulphide deposits formed on continental crust. Geological Journal of China Universities 9 (04), 592–608 in Chinese with English abstract.

Guo, W.M., 2010. Metallogenic mechanism, petrogeochemistry and mineralogy of Dongguashan deposit in Tongling, Anhui Province (doctoral dissertation). Supervisor: Lu J J. Nanjing: Nanjing University (in Chinese).

Han, F., Ge, C.F., 1983. The Makeng iron deposit: a marine volcano-sedimentary deposit. Sci. China (Series B) 438–446 in Chinese with English abstract.

Hannington, M., 2021. VMS and SEDEX Deposits.

He, Y.J., 1990. Metallogenic-geologic characteristics of Yushui Hydrothermal-sedimentary polymetallic deposit in Meixian county. Guangdong Province. Guangdong Geology 5 (1), 1–13 in Chinese with English abstract.

Herzig, P.M., Hannington, M.D., 1995. Polymetallic massive sulfides at the modern seafloor a review. Ore Geology Reviews 10 (2), 95–115.

Hou, Z., Yang, Z., Lu, Q., Zeng, P., Xie, Y., Meng, Y., Tian, S., Xu, W., Li, H., Jiang, Z., Wang, X., Yao, X., 2011. The Large-Scale Dongguashan deposit-Shizishan district in East China: Carboniferous Sedex-type Massive Sulfides Overprinted by Late Jurassic Skarn Cu Mineralization. Acta Geologica Sinica 85 (5), 659–686 in Chinese with English abstract.

Huang, Y., 2015. Metallogenic Mechanism of the massive sulfide deposit formed in the fault depression zones on the continental crust- a case study of the Yushui deposit copper-polymetallic deposit, Eastern Guangdong Province. Sun Yat-sen university (in Chinese), China.

Huang, Y.i., Sun, X., Shi, G., Sa, R., Guan, Y., Jiang, X., Que, H., 2015. Re–Os dating of sulphides from the Yushui Cu-polymetallic deposit in eastern Guangdong Province. South China. Ore Geology Reviews 70. 70, 281–289.

Jia, L., Mao, J., Liu, P., Li, Y., 2018. Petrogenesis of the late Early Cretaceous granodiorite – Quartz diorite from eastern Guangdong, SE China: Implications for tectono–magmatic evolution and porphyry Cu–Au–Mo mineralization. LITHOS 304–307, 388–411.

Jia, L., Mao, J., Liu, P., Yu, M., 2020a. Crust–mantle interaction during subduction zone processes: Insight from late Mesozoic I-type granites in eastern Guangdong, SE China. Journal of Asian Earth Sciences 192, 104284.

Jia, L., Mao, J., Zheng, W., 2020b. Geochronology, geochemistry, and Sr–Nd–Hf–O isotopes of the Zhongqiuyang rhyolitic tuff in eastern Guangdong, SE China: Constraints on petrogenesis and tectonic setting. Geological Journal 55. 55 (7), 5082–5100.

Jia, L., 2018. Petrogenesis of Late Mesozoic granitoids and evalution of metallogenic potential in Eastern Guangdong, coastal area of SE China. China University of Geosciences (Beijing) (in Chinese).

Jiang, B., 2016. Research on geological and geochemical characteristics of YuShui Cu polymetallic deposit in Guangdong. China University of Geosciences (Beijing) (in Chinese).

Jiang, S., Ding, Q., Yang, S., Zhu, Z., Sun, M., Sun, Y., Bian, L., 2011. Discovery and Significance of Carbonate Mud Mounds from Cu-polymetallic Deposits in the Middle and Lower Yangtze Metallogenic Belt: Examples from the Wushan and Dongguashan Deposits. Acta Geologica Sinica 85 (5), 744–756 in Chinese with English abstract.

Jiang, S.Y., Sun, Y., Sun, M.Z., Bian, L.Z., Xiong, Y.G., Yang, S.Y., Cao, Z.Q., Wu, Y.M., 2010. Reiterative fault systems and superimposed mineralization in the Jiurui metallogenic cluster district, Middle and Lower Yangtze River mineralization belt. China. Acta Petrologica Sinica 26 (09), 2751–2767 in Chinese with English abstract.

Jiang, B., Zhu, X., Cheng, X., 2014. Fluid inclusion characteristics and geological significance of Yushui copper deposit in Guangdong Province. Mineral Deposits 33, 513–514 in Chinese with English abstract.

Ke, C., 2021. Spatial-temporal evolution, isotope characteristics of Yanshanian magmatism and their significance in Southeastern Coast of China. Chinese Academy of Geological Sciences (in Chinese).

Koppers, A.A.P., 2002. ArArCALC—software for 40Ar/39Ar age calculations. Computers & Geosciences 28 (5), 605–619.

Li, J., Cai, W.-Y., Li, B., Wang, K.-Y., Liu, H.-L., Konare, Y., Qian, Y.e., Lee, G.-J., Yoo, B.-C., 2019a. Paleoproterozoic SEDEX-type stratiform mineralization overprinted by Mesozoic vein-type mineralization in the Qingchengzi Pb-Zn deposit, Northeastern China. Journal of Asian Earth Sciences 184, 104009.

Li, W., Xie, G.-Q., Mao, J.-W., Cook, N.J., Wei, H.-T., Ji, Y.-H., Fu, B., 2022. Precise age constraints for the Woxi Au-Sb-W deposit, South China. Economic Geology.

Li, X.-H., Li, Z.-X., Li, W.-X., Liu, Y., Yuan, C., Wei, G., Qi, C., 2007. U-Pb zircon, geochemical and Sr–Nd–Hf isotopic constraints on age and origin of Jurassic I- and A-type granites from central Guangdong, SE China: A major igneous event in response to foundering of a subducted flat-slab? LITHOS 96 (1-2), 186–204.

Li, B., Jiang, S.-Y., Lu, A.-H., Lai, J.-Q., Zhao, K.-D., Yang, T., 2016. Petrogenesis of Late Jurassic granodiorites from Gutian, Fujian Province, South China: Implications for multiple magma sources and origin of porphyry Cu–Mo mineralization. LITHOS 264, 540–554.

Li, Z.-X., Li, X.-H., 2007. Formation of the 1300-km-wide intracontinental orogen and postorogenic magmatic province in Mesozoic South China: A flat-slab subduction model. Geology 35, 179–182.

Li, Y.H.M., Zhao, W.W., Zhou, M.-F., 2017. Nature of parent rocks, mineralization styles and ore genesis of regolith-hosted REE deposits in South China: An integrated genetic model. Journal of Asian Earth Sciences 148, 65–95.

Li, M.Y.H., Zhou, M.-F., Williams-Jones, A.E., 2019b. The Genesis of Regolith-Hosted Heavy Rare Earth Element Deposits: Insights from the World-Class Zudong Deposit in Jiangxi Province, South China. Economic Geology 114, 541–568.

Ling, X.X., Li, Q.L., Liu, Y., Yang, Y.H., Liu, Y., Tang, G.Q., Li, X.H., 2016. In situ SIMS Th–Pb dating of bastnaesite: constraint on the mineralization time of the Himalayan Mianning–Dechang rare earth element deposits. Journal of Analytical Atomic Spectrometry 31 (8), 1680–1687.

Liu, P., 2018. The W-Sn metallogeny and its geodynamic setting, eastern Guangdong Province. China University of Geosciences (Beijing) (in Chinese), Southeast Coast.

Liu, P., Gu, X., Zhang, W., Hu, H., Chen, X., Wang, X., Song, W., Yu, M., Cook, N.J., 2023. Jingwenite-(Y) from the Yushui Cu deposit, South China: The first occurrence of a V-HREE-bearing silicate mineral. American Mineralogist 108, 192-196.

Liu, Y., Hu, Z., Gao, S., Günther, D., Xu, J., Gao, C., Chen, H., 2008. In situ analysis of major and trace elements of anhydrous minerals by LA-ICP-MS without applying an internal standard. Chemical Geology 257 (1-2), 34–43.

Liu, Y.S., Hu, Z.C., Zong, K.Q., Gao, C.G., Gao, S., Xu, J., Chen, H.H., 2010. Reappraisement and refinement of zircon U-Pb isotope and trace element analyses by LA-ICP-MS. Chinese Science Bulletin 55 (15), 1535–1546.

Liu, P., Mao, J., Santosh, M., Bao, Z., Zeng, X., Jia, L., 2018. Geochronology and petrogenesis of the Early Cretaceous A-type granite from the Feie'shan W-Sn deposit in the eastern Guangdong Province, SE China: Implications for W-Sn mineralization and geodynamic setting. LITHOS 300–301, 330–347.

Liu, Z.C., Wu, F.Y., Guo, C.L., Zhao, Z.F., Yang, J.H., Sun, J.F., 2011. In situ U-Pb dating of xenotime by laser ablation (LA)-ICP-MS. Chinese Science Bulletin 56 (27), 2948–2956.

Ludwig, K.R., 2003. User's manual for Isoplot/Ex. Version 3.00: a geochronological toolkit for Microsoft Excel. Berkeley Geochronology Center Special Publication, Berkeley, pp. 1–77.

Mao, J., Cheng, Y., Chen, M., Franco, P., 2013. Major types and time–space distribution of Mesozoic ore deposits in South China and their geodynamic settings. Mineralium Deposita 48, 267–294.

Mao, J.W., Shao, Y.J., Xie, G.Q., Zhang, J.D., Chen, Y.C., 2009. Mineral deposit model for porphyry-skarn polymetallic copper deposits in Tongling ore dense district of Middle-Lower Yangtze Valley metallogenic belt. Mineral Deposits 28 (02), 109–119 in Chinese with English abstract.

Mao, J., Zheng, W., Xie, G., Lehmann, B., Goldfarb, R., 2021. Recognition of a Middle-Late Jurassic arc-related porphyry copper belt along the southeast China coast: Geological characteristics and metallogenic implications. Geology 49, 592–596.

Meng, L., Li, Z.-X., Chen, H., Li, X.-H., Wang, X.-C., 2012. Geochronological and geochemical results from Mesozoic basalts in southern South China Block support the flat-slab subduction model. LITHOS 132–133, 127–140.

Ni, P., Tian, J.H., Zhu, X.T., Liang, H.F., Jiang, S.Y., Gu, L.X., 2005. Fluid inclusion studies on footwall stringer system mineralization of Yongping massive copper deposit, Jiangxi province, China. Acta Petrologica Sinica 21, 1339–1346 in Chinese with English abstract.
Pan, Y., Dong, P., 1999. The Lower Changjiang (Yangzi/Yangtze River) metallogenic belt, east central China: intrusion- and wall rock-hosted Cu–Fe–Au, Mo, Zn, Pb, Ag deposits. Ore Geology Reviews 15 (4), 177–242.
Qiu, Z., Yan, Q., Li, S., Wang, H., Tong, L., Zhang, R., Wei, X., Li, P., Wang, L., Bu, A., Yan, L., 2017. Highly fractionated Early Cretaceous I-type granites and related Sn polymetallic mineralization in the Jinkeng deposit, eastern Guangdong, SE China: Constraints from geochronology, geochemistry, and Hf isotopes. Ore Geology Reviews 88, 718–738.
Qiu, W.J., Zhou, M.-F., Li, X., Williams-Jones, A.E., Yuan, H., 2018. The Genesis of the Giant Dajiangping SEDEX-Type Pyrite Deposit, South China. Economic Geology 113, 1419–1446.
Rasmussen, B., Fletcher, I.R., Muhling, J.R., Mueller, A.G., Hall, G.C., 2007. Bushveld-aged fluid flow, peak metamorphism, and gold mobilization in the Witwatersrand basin, South Africa: Constraints from in situ SHRIMP U-Pb dating of monazite and xenotime. Geology 35, 931–934.
Schaarschmidt, A., Haase, K.M., Klemd, R., Keith, M., Voudouris, P.C., Alfieris, D., Strauss, H., Wiedenbeck, M., 2021. Boiling effects on trace element and sulfur isotope compositions of sulfides in shallow-marine hydrothermal systems: Evidence from Milos Island. Greece. Chemical Geology 583, 120457.
Shu, L., Wang, Y., Sha, J., Jiang, S., Yu, J., Wang, Y., 2009. Jurassic sedimentary features and tectonic settings of southeastern China. Science in China Series D: Earth Sciences 52, 1969–1978.
Steiger, R.H., Jager, E., 1977. Subcommission on geochronology: convention on the use of decay constants in geo- and cosmochronology. Earth Planet. Sci. Lett. 36 (3), 359–362.
Tang, Y., Xie, Y., Liu, L., Lan, T., Yang, J., Sebastien, M., Yin, R., Liang, S., Zhou, L., 2017. U-Pb, Re–Os and Ar–Ar dating of the Linghou polymetallic deposit, Southeastern China: Implications for metallogenesis of the Qingzhou-Hangzhou metallogenic belt. Journal of Asian Earth Sciences 137, 163–179.
Tang, Y., Liu, N.a., Yang, J., Gonçalves, G.O., Liu, L., Lan, T., Gao, J., Han, J., 2022. A new calibrated strategy for the in situ U-Th–Pb dating of bastnasite by xenotime. Journal of Analytical Atomic Spectrometry 37 (12), 2599–2614.
Tian, Y., 2020. Jurassic porphyry deposits and crust-mantle interaction along the southeast coast of China: A case study of Gutian porphyry Cu-Mo deposit. Chinese Academy of Geological Sciences (in Chinese).
Vasconcelos, A.D., Gonçalves, G.O., Lana, C., Buick, I.S., Kamo, S.L., Corfu, F., Scholz, R., Alkmim, A., Queiroga, G., Nalini Jr, H.A., 2018. Characterization of Xenotime From Datas (Brazil) as a Potential Reference Material for In Situ U-Pb Geochronology. Geochemistry, Geophysics, Geosystems 19, 2262–2282.
Wang, X., 2015. Preliminary study on geological characteristics and genesis of the Xinliaodong Cu polymetallic deposit in eastern Guangdong province. China University of Geosciences (Beijing) (in Chinese), China.
Wang, X., Mao, J., Cheng, Y., Liu, P., Zhang, X., 2016. Zircon U-Pb age, geochemistry and Hf isotopic compositions of quartzdiorite from the Xinliaodong Cu polymetallic deposit in eastern Guangdong Province. Geological Bulletin of China 35 (8), 1357–1375 in Chinese with English abstract.
Wang, L., Yang, M., Peng, S., 1999. On the genesis of the Yushui polumetallic deposit in the Meixian county, Guangdong Province. Geotectonica et Metallogenia 04, 345–352 (in Chinese with English abstract).
Xie, Y., Hou, Z., Goldfarb, R.J., Guo, X., Wang, L., Verplanck, P.L., Hitzman, M.W., 2016. Rare Earth Element Deposits in China, Rare Earth and Critical Elements in Ore Deposits. Society of Economic Geologists.
Xu, X., 1993. Rare earth element geochemical studies on the Mesozoic volcanic-intrusive complexes in Eastern Guangdong district. Journal of Hefei University of Technology (Natural Science) 16 (2), 121–127 in Chinese with English abstract.
Xu, C., Xie, Q., Yue, S., 2000. Metallogenetic mechanism of Mesozoic metallic ore deposits in eastern Guangdong area. Journal of Hefei University of Technology (Natural Science) 23 (1), 99–103 in Chinese with English abstract.
Xu, C., Kynický, J., Smith, M.P., Kopriva, A., Brtnický, M., Urubek, T., Yang, Y., Zhao, Z., He, C., Song, W., 2017. Origin of heavy rare earth mineralization in South China. Nature Communications 8, 14598.
Xu, G., Zhou, J., 2001. The Xinqiao Cu–S–Fe–Au deposit in the Tongling mineral district, China: synorogenic remobilization of a stratiform sulfide deposit. Ore Geology Reviews 18 (1-2), 77–94.
Xu, K.Q., Zhu, J.C., 1978. Origin of the sedimentary-(or volcanosedimentary-) iron–copper deposits in some fault depression belts in Southeast China. Fujian Geology 4, 1–68 in Chinese with English abstract.
Yang, Y.-L., Ni, P., Pan, J.-Y., Wang, G.-G., Xu, Y.-F., 2017. Constraints on the mineralization processes of the Makeng iron deposit, eastern China: Fluid inclusion, H-O isotope and magnetite trace element analysis. Ore Geology Reviews 88, 791–808.
Yang, Y.-H., Wu, F.-Y., Li, Y., Yang, J.-H., Xie, L.-W., Liu, Y., Zhang, Y.-B., Huang, C., 2014. In situ U-Pb dating of bastnaesite by LA-ICP-MS. Journal of Analytical Atomic Spectrometry 29 (6), 1017–1023.
Yue, X., Liu, L., Zhang, Z., Zhao, Z., Sun, J., Zhao, Y., 2022. Petrogenesis of the Jurassic Representative Volcanic Rocks in Eastern Guangdong: Response to the Early Stage of the Paleo-Pacific Subduction. Geological Journal of China Universities 28, 199–210 in Chinese with English abstract.
Zaw, K., Peters, S.G., Cromie, P., Burrett, C., Hou, Z., 2007. Nature, diversity of deposit types and metallogenic relations of South China. Ore Geology Reviews 31 (1-4), 3–47.
Zhai, Y.S., Wang, J.P., Peng, R.M., Liu, J.J., 2009. Research on superimposed metallogenic systems and polygenetic mineral deposits. Earth Science Frontiers 16 (6), 282–290 (in Chinese with English abstract).
Zhang, Y., Chen, W., Chen, K., Liu, X., 2006. Study on the Ar-Ar age spectrum of diagenetic I/S and the mechanism of ^{39}Ar recoil loss Examples from the clay minerals of P-T boundary in Changxing. Zhejiang Province. Geological Review 52 (4), 556–561.
Zhang, S.M., Xiao, Y.F., Wang, Q., Zhang, X.H., Yang, L., Wang, Y.L., Zhang, C.M., 2013. Re-Os dating of molybdenite from the Tongcun porphyry molybdenum deposit in western Zhejiang Province and its geological implications. Geology and Exploration 49 (1), 50–57.
Zhao, X., Li, L., Xu, M., Liu, H., Zhu, Q., Jin, G., Jiang, Y., 2021. Control of basement on Paleozoic mineralizations in the Wuyi metallogenic belt. Ore Geology Reviews 131, 104037.
Zhao, Z., Wang, D., Bagas, L., Chen, Z., 2022. Geochemical and REE mineralogical characteristics of the Zhaibei Granite in Jiangxi Province, southern China, and a model for the genesis of ion-adsorption REE deposits. Ore Geology Reviews 140, 104579.
Zhou, X.M., Li, W.X., 2000. Origin of Late Mesozoic igneous rocks in Southeastern China: implications for lithosphere subduction and underplating of mafic magmas. Tectonophysics 326 (3-4), 269–287.
Zhou, X., Sun, T., Shen, W., Shu, L., Niu, Y., 2006. Petrogenesis of Mesozoic granitoids and volcanic rocks in South China: A response to tectonic evolution. Episodes 29 (1), 26–33.
Zhu, X.-T., Ni, P., Wang, G.-G., Cai, Y.-T., Chen, H., Pan, J.-Y., 2016. Fluid inclusion, H-O isotope and Pb–Pb age constraints on the genesis of the Yongping copper deposit, South China. Journal of Geochemical Exploration 171, 55–70.

Further reading

Li, S., Chen, H., Peng, Y., Wang, L., Luo, Z., 2019c. Tectonic evolution of the Yongmei depression constrained by zircon LA-ICP-MS U-Pb ages of granite porphyry and diabase from the Yushui Cu-Pb-Zn polymetallic deposit. Geochimica 48, 313–324 in Chinese with English abstract.